American Journal of Modern Physics
2026, Vol. 15, No. 6, pp. 181–194
https://doi.org/10.11648/j.ajmp.20261506.11

SciencePG
Science Publishing Group

Research Article

Influence of the Peclet Number on Heat and Mass Transfer and Droplet Lifetime During Subcritical Iso-octane and Methanol Droplet Evaporation

Yendoubouame Lare[1, *], **Koffi Sagna**[1, 2]

[1]Department of Physics, University of Lomé, Lomé, Togo

[2]Regional Center of Excellence for Electricity Master (CERME), University of Lomé, Lomé, Togo

Abstract

This study investigates the influence of the Peclet number on heat and mass transfer structures and droplet lifetime during the subcritical evaporation of methanol and iso-octane droplets. An analytical model based on the Navier–Stokes and energy conservation equations is developed to describe transport phenomena in the liquid and surrounding gas phases. Using an asymptotic expansion approach, zeroth- and first-order analytical expressions for the temperature and density fields are obtained and used to characterize thermo-mass transfer mechanisms during droplet evaporation. Three Peclet numbers, 5, 0.5, and 0.005 are considered to examine the transition between transport regimes with different relative contributions of convective and diffusive mechanisms. The results indicate that the magnitude and spatial distribution of the thermal and density perturbations near the liquid–vapor interface depend on the Peclet number. Variations in the Peclet number modify the structure of the temperature and density fields in both the liquid and gas regions. The droplet regression curves also show a dependence of evaporation lifetime on this parameter, highlighting the role of transport mechanisms in determining droplet evolution. The comparison between methanol and iso-octane reveals distinct thermo-mass transfer behaviors for the two fluids, reflecting the influence of their thermophysical characteristics on the evaporation process. Further analysis shows that transport regimes affect not only local field distributions but also the overall evaporation dynamics. By combining the analysis of thermal fields, density distributions, and droplet regression, this study provides a comparative assessment of the relationship between transport regimes and evaporation dynamics within the adopted analytical model. The results contribute to a better understanding of heat and mass transfer during subcritical droplet evaporation.

Keywords

Peclet Number, Navier–Stokes Equations, Evaporation, Droplet Lifetime, Subcritical

1. Introduction

Fuel droplet evaporation is a fundamental process in numerous energy applications, including diesel engines, gas turbines, and space propulsion systems. The performance of these devices strongly depends on fuel heating, vaporization, and mix-

*Correspondence: Yendoubouame Lare (ylare1509@outlook.com)

Received: 15 October 2026; **Accepted:** 29 October 2026; **Published:** 23 November 2026

Copyright: © The Author(s), 2026. Published by Science Publishing Group. This is an **Open Access** article, distributed under the terms of the Creative Commons Attribution 4.0 License (http://creativecommons.org/licenses/by/4.0/), which permits unrestricted use, distribution and reproduction in any medium, provided the original work is properly cited.

ing processes with the surrounding medium. A precise description of heat and mass transfer mechanisms around evaporating droplets is therefore essential for improving combustion efficiency and reducing pollutant emissions. Numerous studies have investigated droplet evaporation under subcritical conditions. In particular, the review by Sazhin [1] provides a comprehensive overview of the main models developed to describe fuel droplet heating and evaporation.

The first theoretical models of droplet evaporation were proposed by Maxwell [2] and later extended by Spalding [3] and Godsave [4] through the establishment of the classical d^2-law. This theory predicts a linear decrease of the squared droplet diameter with time under quasi-steady evaporation conditions. Although widely used, this approach relies on several simplifying assumptions whose validity has been questioned by numerous experimental and numerical studies. Significant deviations from classical theory have been reported in the presence of strong thermal gradients, convective effects, or variations in thermophysical properties [5, 6].

More recently, several investigations have revealed the existence of complex thermo-mass transfer structures near the liquid–vapor interface. Sagna et al. [7, 8] showed the emergence of thermal and mass waves associated with discontinuities in temperature and density fields. These phenomena reflect the strong coupling between heat and mass transfer processes and may significantly affect both evaporation dynamics and droplet lifetime. They may also promote incomplete combustion and consequently increase pollutant emissions [9, 10].

Although previous studies have established analytical formulations for droplet evaporation under subcritical conditions, a systematic comparison of the influence of the Peclet number on the predicted thermal fields, density fields, and droplet lifetime for methanol and iso-octane remains to be clarified within the framework considered here. In particular, the relationship between the spatial distribution of thermo-mass perturbations near the liquid–vapor interface and the overall droplet regression requires further examination.

The present study therefore investigates the influence of three Peclet numbers (P_e *5, 0.5 and 0.005*) on the evaporation of methanol and iso-octane droplets under subcritical conditions. The analytical expressions established in previous work are used to compare the temperature and density fields in the liquid and gas phases and to examine their relationship with droplet regression and lifetime. The contribution of this study lies in the comparative parametric analysis of these quantities for the two fluids, rather than in claiming the development of an entirely new analytical model. The analysis addresses three questions: (i) How does the Peclet number affect the amplitude and spatial distribution of thermal and density perturbations? (ii) How do the predicted fields differ between methanol and iso-octane under the conditions considered? and (iii) How does the Peclet number affect the droplet regression rate and the resulting lifetime?

The results are interpreted in relation to the assumptions and range of validity of the analytical model. Attention is paid to distinguishing trends directly obtained from the analytical solutions from physical interpretations that require additional quantitative evidence.

2. Mathematical formulation

A pure iso-octane or methanol droplet, initially at the saturation temperature corresponding to the considered subcritical pressure, is instantaneously introduced into an infinite gaseous environment at a higher temperature and initially at rest. At the initial time, the droplet radius, density, and temperature are denoted by $R'(0) = R'_{in}(m), \rho'(0) = \rho'_{in}$ et $T'(0) = T'_{in}$, respectively. The surrounding medium is characterized by its temperature T_∞ (K), pressure $P_\infty(Pa)$, and density $\rho_\infty(Kg/m\text{^}3)$.

The mathematical model is based on the following assumptions:

1) the droplet maintains a spherical shape throughout the evaporation process;
2) the fluid is Newtonian and compressible;
3) the flow is spherically symmetric;
4) the process is isobaric, with a uniform pressure field;
5) radiative heat transfer is neglected;
6) The surrounding gas is initially at rest, with no natural or forced convection;
7) Soret and Dufour thermo-diffusion effects are neglected;
8) thermodynamic equilibrium is maintained at the liquid–vapor interface;
9) the thermodynamic conditions remain subcritical throughout the process.

The radial coordinate is denoted by r, while $R(t)$ represents the instantaneous droplet radius. The fluid is assumed to behave as an ideal gas, and the flow field is described by the radial velocity u. Under these assumptions, the evolution of the system is governed by the conservation equations of mass, momentum, and energy:

$$\begin{cases} \dfrac{\partial \rho'}{\partial t'} + \dfrac{1}{r'^2}\dfrac{\partial\left(r'^2 \rho' v'\right)}{\partial r'} = 0 \\ \rho'\left(\dfrac{\partial v'}{\partial t'} + v'\dfrac{\partial v'}{\partial r'}\right) = 0 \\ \dfrac{\partial T'}{\partial t'} + v'\dfrac{\partial T'}{\partial r'} = \dfrac{1}{\rho' C'_p r'^2}\dfrac{\partial\left(r'^2 \lambda' \frac{\partial T'}{\partial r'}\right)}{\partial r'} \end{cases} \quad (1)$$

To facilitate the tracking of the moving liquid-gas interface, the governing equations are rewritten in a moving coordinate system defined by $x' = r' - R'$.

Two characteristic time scales are introduced: the thermal diffusion time t'_{dif} and the droplet lifetime t'_{res}. Characteristic velocity scales are also defined $U'_l = \frac{R'_{in}}{t'_{res}}$ and $U'_g = \frac{R'_{in}}{t'_{dif}}$. Furthermore, the characteristic densities ρ'_l and ρ'_∞ are used to represent the liquid and gaseous phases, respectively.

The nondimensionalization of the governing equations leads to the following dimensionless parameters:

$$\varepsilon = \frac{\rho'_\infty}{\rho'_l},\ P_e = \frac{C'_{p\infty}\rho'_\infty R'^2_{in}}{\lambda'_\infty\ t'_{dif}},\ \gamma_\infty = \frac{t'_{dif}}{t'_{res}},\ \tau = \frac{\gamma_\infty}{\varepsilon} \tag{2}$$

together with the associated dimensionless variables:

$$t' = t'_{res}t, \quad R' = R'_{in}r_o, \quad x' = R'_{in}x$$

$$u' = U'_g u, \dot{R}' = U'_l\ \dot{r}_o, \quad T' = T'_\infty T, \tag{3}$$

$$\rho' = \rho'_\infty\tilde{\rho}\ \rho' = \rho'_l\bar{\rho},\ P' = P'_\infty P.$$

Substituting these variables into the conservation equations yields the dimensionless system governing droplet evaporation [11]:

$$\begin{cases} \frac{\gamma_\infty}{\varepsilon}\left(\frac{\partial\bar{\rho}}{\partial t} + \frac{2\bar{\rho}\dot{r}_0}{x+\ r_0} + \dot{r}_0\frac{\partial\bar{\rho}}{\partial x}\right) + \frac{1}{(x+\ r_0)^2}\frac{\partial[(x+\ r_0)^2\tilde{\rho}u]}{\partial x} = 0 \\ \frac{\gamma_\infty}{\varepsilon}\bar{\rho}\left(\frac{\partial u}{\partial x}\dot{r}_0 + \ \tau_\infty\ddot{r}_0\right) + \tilde{\rho}\left(\gamma_\infty\frac{\partial u}{\partial t} + u\frac{\partial u}{\partial x}\right) = -\frac{P_\infty t^2_{dif}}{R^2_{in}\rho_\infty}\frac{\partial p}{\partial x} \\ \frac{\gamma_\infty}{\varepsilon}\left(\frac{\partial T}{\partial t} + \dot{r}_0\frac{\partial T}{\partial x}\right) + u\frac{\partial T}{\partial x} = \frac{1}{P_e\tilde{\rho}C_p(x+\ r_0)^2}\frac{\partial\left[\lambda(x+\ r_0)^2\frac{\partial T'}{\partial x'}\right]}{\partial x} \end{cases} \tag{4}$$

In terms of the dimensionless variables, the initial conditions become:

$$T(0,x) = \begin{cases} T_{in}(x), x \le 0 \\ T_\infty(x), x > 0 \end{cases}$$

$$\rho(0,x) = \begin{cases} \rho_{in}(x), x \le 0 \\ \rho_\infty(x), x > 0 \end{cases} \tag{5}$$

$$u(0,x) = \begin{cases} u_{in}(x), x \le 0 \\ u_\infty(x), x > 0 \end{cases}$$

The boundary conditions are written as:

$$T(t,x) = T_l(t), x \le 0 \quad \lim_{x\to+\infty} T(t,x) = \ T_\infty(t)$$

$$\rho(t,x) = \rho_l(t), x \le 0 \quad \lim_{x\to+\infty}\rho(t,x) = \rho_\infty(t) \tag{6}$$

$$u(t,x) = u_l(t), x \le 0 \quad \lim_{x\to+\infty} u(t,x) = u_\infty(t)$$

The jump conditions at the liquid-gas interface take the following dimensionless form:

$$\lambda_l\left(\frac{\partial T}{\partial x}\right)_l + P_e\rho_l u_l\mathcal{L}_0 = \ \lambda_g\left(\frac{\partial T}{\partial x}\right)_g, \quad \mathcal{L}_0 = \frac{h'_l - h'_g}{C_{p\infty}T_\infty} \tag{7}$$

where h' denotes the total enthalpy associated with the relative motion.

Dimensionless parameter naturally appears in the governing system, namely $\Pi = \frac{P_\infty t^2_{dif}}{R^2_{in}\rho_\infty}$. This parameter compares the mechanical effects associated with pressure to the thermal diffusion mechanisms. It measures the ratio between the characteristic thermal diffusion time and the characteristic time associated with the propagation of pressure disturbances within the fluid. When Π is small, mechanical effects remain secondary compared with diffusive transport processes, and the flow evolution is mainly governed by heat transfer mechanisms. Conversely, as Π increases, pressure effects exert a stronger influence on the flow dynamics, and the coupling between thermal and mechanical phenomena becomes more significant. In classical dimensional analyses reported in the literature [12, 13], only the parameters ε or γ_∞ are generally used to characterize the quasi-steady regime. The present formulation, however, highlights the complementary role of the parameter Π, which accounts for the influence of pressure effects on the evolution of the system. Furthermore, examination of the dimensionless system shows that the unsteady terms appearing in the mass and energy conservation equations are governed by the parameter $\tau = \frac{\gamma_\infty}{\varepsilon}$. In the momentum conservation equation, τ also controls the terms associated with the temporal variation of the droplet radius. When $\tau \to 0$, the governing system tends toward a quasi-steady regime. An asymptotic expansion in powers of τ can then be performed, leading to the first- and second-order systems of equations [7, 8, 14]. The parameter τ characterizes the asymptotic ordering adopted in the present formulation.

First approximation system Eq (8):

$$\begin{cases} \frac{1}{(x+r_o)^2}\frac{\partial[(x+r_o)^2\rho_0 u_0]}{\partial x} = 0 \\ \rho_0\left(\gamma_\infty\frac{\partial u_0}{\partial t} + u_0\frac{\partial u_0}{\partial x}\right) = 0 \\ u_0\frac{\partial T_0}{\partial x} = \ \frac{1}{P_e C p_0(x+r_o)^2}\frac{\partial\left[(x+r_o)^2\lambda_0\frac{\partial T_0}{\partial x}\right]}{\partial x} \end{cases} \tag{8}$$

Second approximation system Eq. (9):

$$\begin{cases} \frac{1}{(x+r_o)^2}\frac{\partial[(x+r_o)^2(\rho_1 u_0 + \rho_0 u_1]}{\partial x} = 0 \\ \rho_0\left(\gamma_\infty\frac{\partial u_1}{\partial t} + u_0\frac{\partial u_1}{\partial x} + u_1\frac{\partial u_0}{\partial x}\right) + \rho_1\left(\gamma_\infty\frac{\partial u_0}{\partial t} + u_0\frac{\partial u_0}{\partial x}\right) = 0 \\ \left(\frac{\partial T_1}{\partial t} + \frac{\partial T_0}{\partial x}\dot{r}_0 + u_0\frac{\partial T_1}{\partial x} + u_1\frac{\partial T_0}{\partial x}\right) = \ \frac{1}{P_e C p_0(x+r_o)^2}\frac{\partial\left[(x+r_o)^2(\lambda_0\frac{\partial T_1}{\partial x} + \lambda_1\frac{\partial T_0}{\partial x})\right]}{\partial x} \\ \qquad - \frac{(\rho_0 C p_1 + \rho_1 C p_0)}{P_e C p_0(x+r_o)^2}\frac{\partial\left[(x+r_o)^2\lambda_0\frac{\partial T_0}{\partial x}\right]}{\partial x} \end{cases} \tag{9}$$

where:

1) ρ_0, ρ_1 are zeroth- and first-order density perturbations.
2) u_0, u_1 are zeroth- and first-order velocity perturbations.
3) T_0, T_1 are zeroth- and first-order temperature perturbations.
4) P_0, P_1 are zeroth- and first-order pressure perturbations.

In the remainder of the study, the heat capacity $Cp_0(x,t) = Cp_0(t)$ and the thermal conductivity $\lambda_0(x,t) = \lambda_0(t)$ are assumed to be uniform and independent of the distance x. The assumption of uniform pressure allows for the decoupling of the system of conservation equations, enabling the velocity, density, and temperature fields to be treated separately. The solutions are constrained by the conditions imposed at the droplet center, the liquid–vapor interface, and the far field. These conditions are applied consistently to determine the unknown constants.

Table 1 summarizes the thermophysical properties and operating conditions parameters used in the calculations. The same parameter definitions are used consistently when comparing methanol and iso-octane.

Table 1. *Thermophysical properties and operating conditions used in the analytical model.*

Parameter	Symbol	Unit	Methanol	Iso-octane
Initial droplet radius	R_0	µm	15	15
Initial droplet temperature	$T_{d,0}$	K	288	288
Ambient gas temperature	T_∞	K	480	480
Operating pressure	P	atm	1	1
Liquid density	ρ_l	kg m^{-3}	791	692
Specific heat capacity	C_p	J kg^{-1} K^{-1}	2535	2220
Thermal conductivity	λ_0	W m^{-1} K^{-1}	0.200	0.137
Latent heat	$\mathcal{L}_0$	kJ kg^{-1} ·	1100	305

3. Analytical Resolution

3.1. Velocity Field

The asymptotic solution of the momentum equation yields the following expressions for the zero- and first-order approximations of the velocity field:

$$\begin{cases} u_0(x,t) = \frac{\gamma_\infty(a_0 x + a_1)}{a_0 t + \gamma_\infty a_2} \\ u_1(x,t) = \frac{u_0(x,t)}{\gamma_\infty(a_0 t + \gamma_\infty a_2)} \end{cases} \quad (10)$$

where a_0, a_1 and a_2 are constant. The solution (10) makes it possible to consider the variation of the relative velocity as a function of x the drop and/or the gaseous phase. According to Koffi Sagna *et al*. works [10], the constants a_0, a_1 and a_2 are determined by the boundary conditions on the interface.

3.2. Density Field

Substituting the velocity solution into the continuity equation leads to the following expressions for the density field:

$$\begin{cases} \rho_0(x,t) = \frac{f(t)}{u_0(x,t)(x+r_0)^2} \\ \rho_1(x,t) = \frac{1}{u_0(x,t)(x+r_0)^2}\left[g(t) - \frac{f(t)}{\gamma_\infty(a_0 t + \gamma_\infty a_2)}\right] \end{cases} \quad (11)$$

The solutions obtained show that the evolution of mass density is directly linked to the velocity distribution within the liquid and gaseous phases. They thus make it possible to describe the effects of spatial variations in the velocity field on the dynamics of evaporation.

3.3. Temperature Field

The temperature field is determined from the third equation in systems (8) and (9). Integrating the energy equations then leads to the following relations:

$$\begin{cases} T_0(x,t) = \frac{k(t)}{P_e Cp_0(t) f(t)} \exp\left[\frac{P_e Cp_0 f(t)}{\lambda_0}\left(\frac{1}{r_0} - \frac{1}{x+r_0}\right)\right] + \phi(t) \\ T_1(x,t) = \frac{k}{P_e Cp_0 f}\left[\frac{q(t)}{k} + \alpha\left(\frac{1}{r_0} - \frac{1}{x+r_0} - \frac{\lambda_0}{P_e Cp_0 f}\right) + \beta\left(\frac{a_0}{2}x^2 + a_1 x\right)\right] exp\left(\frac{P_e Cp_0 f}{\lambda_0}\left(\frac{1}{r_0} - \frac{1}{x+r_0}\right)\right) \\ + \frac{\lambda_0 k\alpha}{(P_e Cp_0 f)^2} - \frac{\beta k}{P_e Cp_0 f}\left(\frac{a_0}{2}x^2 + a_1 x\right) exp\left(\frac{P_e Cp_0 f}{\lambda_0 r_0}\right) \end{cases} \quad (12)$$

With

$$B(l,t) = \left(\frac{1}{r_0} - \frac{1}{l+r_0}\right)\frac{k(t)}{(l+r_o)^2} \exp\left[\frac{P_e Cp_0 f(t)}{\lambda_0}\left(\frac{1}{r_0} - \frac{1}{l+r_0}\right)\right]$$

$$A(l,t) = \frac{k(t)}{P_e Cp_0(t) f(t)}\left(\frac{\frac{a_0}{2}l^2 + a_1 l}{(l+r_0)^2}\right) \exp\left[\frac{P_e Cp_0 f(t)}{\lambda_0}\left(\frac{1}{r_0} - \frac{1}{l+r_0}\right)\right] \quad (13)$$

$$\alpha(t) = \frac{P_e Cp_0(t) f(t)}{\lambda_0(t)\gamma_\infty(a_0 t + \gamma_\infty a_2)}$$

$$\beta(t) = \frac{P_e}{\lambda_0(t)(a_0 t + \gamma_\infty a_2)}\left[\frac{\gamma_\infty g(t)}{f(t)} - \frac{1}{(a_0 t + \gamma_\infty a_2)}\right]$$

The functions $k(t), q(t)$ and $\phi(t)$ are determined using the boundary conditions and they are:

$$k(t) = \frac{P_e Cp_0 f(t)(T_0^0 - T_0^\infty)}{1 - exp\left(\frac{P_e Cp_0 f(t)}{\lambda_0 r_0}\right)}$$

$$\phi(t) = \frac{T_0^\infty - T_0^0 exp\left(\frac{P_e Cp_0 f(t)}{\lambda_0 r_0}\right)}{1 - exp\left(\frac{P_e Cp_0 f(t)}{\lambda_0 r_0}\right)} \quad (14)$$

$$q(t) = \frac{P_e Cp_0 f(T_0^0 - T_0^\infty)}{1 - exp\left(\frac{P_e Cp_0 f}{\lambda_0 r_0}\right)}\left(\varepsilon + \frac{1}{\gamma_\infty(a_1 t + \gamma_\infty a_3)}\right)$$

with $T_0^0(t) = T_0(t,0)$ and $\lim_{x\to+\infty} T_0(t,x) = T_0^\infty(t)$.

The integration constants were determined by applying the liquid-vapor interface continuity conditions and the far-field boundary conditions. The solutions obtained describe the spatial and temporal evolution of the temperature field at the zeroth and first orders. They highlight the influence of heat transfer on the structure of the thermal field in the vicinity of the liquid-gas interface.

3.4. Droplet Regression Law

We integrate the third equations of the Eq (8) and (9) and we find (15):

$$\begin{cases} \lambda_0(x,t)\frac{\partial T_0(x,t)}{\partial x} = \frac{k(t)}{(x+r_o)^2} \exp\left[P_e \int_0^x \frac{Cp_0 \rho_0 u_0}{\lambda_0}(a,t)da\right] \\ \frac{\partial T_1(x,t)}{\partial x} = \left[\frac{q}{k} + \frac{P_e}{\lambda_0}\left(\beta\left(\frac{a_0}{2}x^2 + a_1 x\right) + \alpha\left(\frac{1}{r_0} - \frac{1}{x+r_0}\right)\right)\right]\frac{\partial T_0(x,t)}{\partial x} \end{cases} \quad (15)$$

Considering that the drop is at rest, we obtain $u_{0g} = -\gamma_\infty \dot{r_0}$ and apply the jump relations (7) to equation (15) we obtain (16):

$$\begin{cases} \rho_{0g} u_{0g} = -\tau \rho_{0l} \dot{r_0} \\ P_e \rho_{0l} u_{0l} \mathcal{L}_0 = \lambda_{0g}\left(\frac{\partial T_0}{\partial x}\right)_{0g} \\ P_e(\rho_{0l} u_{1l} + \rho_{1l} u_{0l})\mathcal{L}_0 = \lambda_{0g}\left(\frac{\partial T_1}{\partial x}\right)_{0g} \end{cases} \quad (16)$$

The relations (11) written on the boundary of the drop considering the relation (15) give (17):

$$f(t) = -\tau \rho_{0l} r_0^2 \dot{r_0} = \frac{k}{P_e \mathcal{L}_0} \quad (17)$$

$$g(t) = -\tau \rho_{0l} r_0^2 \dot{r_0}\left(\epsilon + \frac{1}{\gamma_\infty(a_0 t + \gamma_\infty a_2)}\right) = \frac{q}{P_e \mathcal{L}_0}$$

The relation (17) gives the differential equation which describes the drop's radius evolution versus time. The integration of (19) gives a recession law d^3 for the diameter of the drop with a nonlinear function of time [16]. To determine the evolution of the temperature we must know the functions $k(t)$ and $q(t)$ regarding equation (15).

The evolution of the droplet radius during evaporation is obtained from the interfacial energy balance and the resulting mass loss rate. The asymptotic formulation leads to the following expressions for the zeroth-order and first-order droplet regression laws:

$$r_0^2 = 1 - \frac{2}{\tau P_e \rho_{0l}} \int_0^t \frac{\lambda_0(\xi)}{Cp_0(\xi)} \ln\left(1 + \frac{Cp_0(\xi)}{\mathcal{L}_0}(T_0^\infty - T_0^0)\right) d\xi \quad (18)$$

$$r_1^2 = 1 - \frac{2}{\tau P_e \rho_{0l}} \int_0^t \frac{\lambda_0(\xi)}{Cp_0(\xi)} \left[\frac{\ln\left(1 + \frac{Cp_0(\xi)}{\mathcal{L}_0 \varepsilon}(T_0^\infty - T_0^0)\right)}{\left(1 + \frac{1}{\gamma_\infty \varepsilon(a_0 \xi + \gamma_\infty a_2)}\right)}\right] d\xi \quad (19)$$

These expressions generalize classical recession laws and show that the evolution of the radius depends directly on the thermophysical properties of the fluid as well as on the dimensionless parameters of the problem.

4. Results and Discussion

Although the analytical solutions were previously established, the influence of the Peclet number on thermal and mass transfer structures and on droplet lifetime has not yet been investigated. The present section focuses on this aspect for methanol and iso-octane droplets under subcritical conditions. Three values of the Peclet number (5, 0.5 and 0.005) were selected to represent convection-dominated, mixed convection-diffusion and diffusion-dominated transport regimes, respectively.

4.1. Thermal Field Model

Figures 1–12 show the T_0 and T_1 temperature profiles obtained for methanol and iso-octane droplets at different Peclet numbers ($Pe = 5$, $Pe = 0.5$, and $Pe = 0.005$). These results reveal the formation of thermal waves localized near the liquid–vapor interface. The intensity of these waves strongly depends on the Peclet number. For large values of Pe, the thermal gradients are high and concentrated within a narrow region around the interface. As Pe decreases, these gradients progressively weaken and the region affected by heat transfer becomes wider. Diffusive mechanisms then become dominant, promoting a more homogeneous redistribution of heat within the droplet [15]. Similar observations have been reported by Sazhin [1] and Sirignano [16] in their studies on the heating and evaporation of fuel droplets. The differences observed between methanol and iso-octane also reflect the influence of the fluid thermophysical properties on the structure of the thermal field. The following sections provide a detailed analysis of the T_0 and T_1 profiles for the various transport regimes considered.

4.1.1. Analysis of Temperature Gradients T_0 and T_1 for $Pe = 5$

The T_0 and T_1 profiles exhibit pronounced peaks near the liquid–vapor interface, indicating the presence of thermal waves associated with the phase-change process. The amplitudes observed for iso-octane are higher than those of methanol, indicating stronger thermal gradients and a greater concentration of heat transfer at the interface. This difference is related to the thermophysical properties of the two fuels. Due to its higher volatility, methanol promotes a more uniform thermal diffusion, whereas iso-octane develops steeper gradients because of the larger energy input required for its evaporation. Similar behaviors have been reported by Schwarz et al. [17] and Abramzon and Sirignano [18].

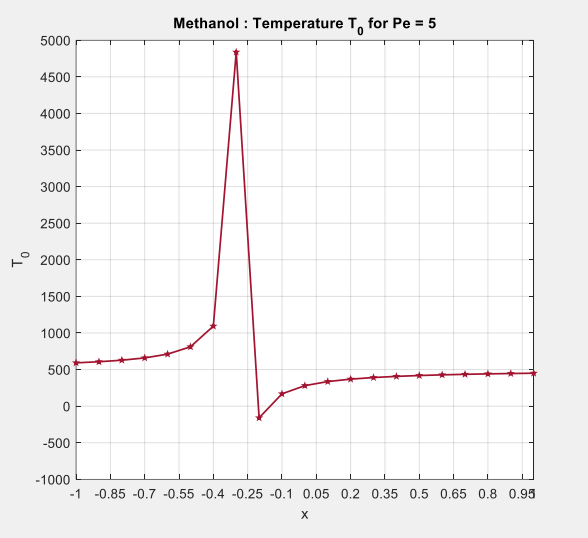

Figure 1. *$T_0(x)$ temperature profile of methanol for $P_e = 5$.*

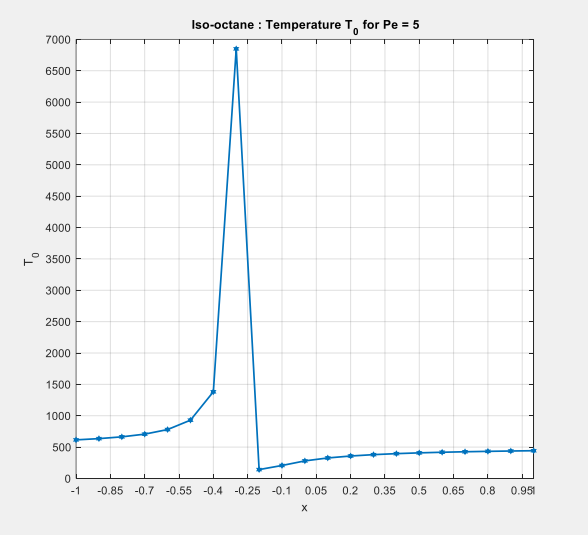

Figure 2. *$T_0(x)$ temperature profile of iso-octane for $P_e = 5$.*

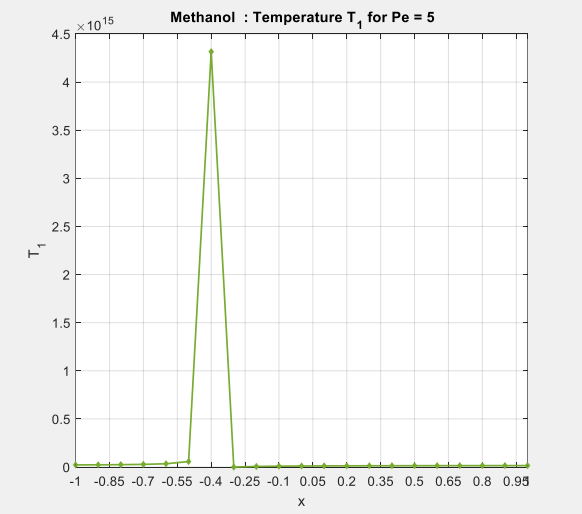

Figure 3. *$T_1(x)$ temperature profile of methanol for $P_e = 5$.*

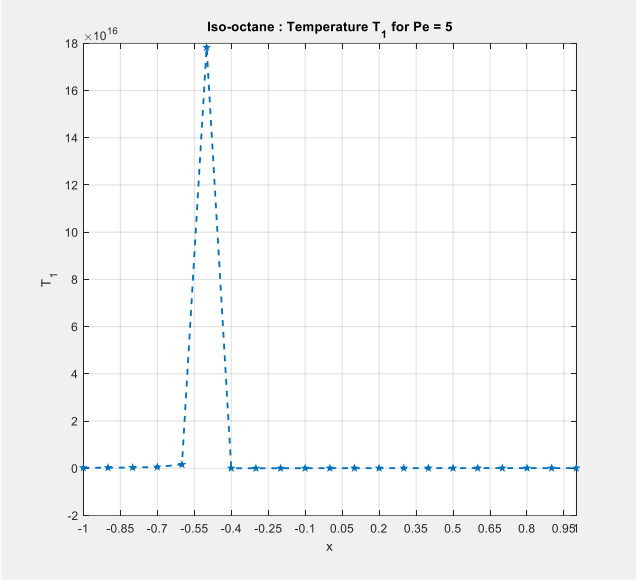

Figure 4. *$T_1(x)$ temperature profile of iso-octane for $P_e = 5$.*

The T_1 profiles confirm the trends observed for T_0, but with higher amplitudes, highlighting the importance of first-order effects in the thermal dynamics of evaporation. These results show that, at $Pe = 5$, convective mechanisms dominate diffusion processes and promote the development of intense thermal waves, particularly in the case of iso-octane. This observation is consistent with the findings of Pinheiro and Vedovoto [19], who showed that stronger convective effects tend to increase the concentration of thermal gradients in the immediate vicinity of droplet surfaces.

4.1.2. Analysis of Temperature Gradients T_0 and T_1 for $Pe = 0.5$

The T_0 and T_1 profiles also exhibit localized peaks near the liquid–vapor interface. However, compared with the $Pe = 5$ case, these peaks are less intense and more spatially spread, particularly for methanol. This behavior reflects the increasing influence of diffusive mechanisms as the Peclet number decreases below unity. The reduction in Pe weakens the concentration of heat transfer at the interface and promotes heat redistribution over a wider region surrounding the droplet. As a result, thermal gradients decrease in amplitude while the thickness of the thermal boundary layer increases. This effect is more pronounced for methanol, whose profiles become more diffuse, whereas iso-octane still exhibits relatively strong gradients, although less intense than those observed at $Pe = 5$.

The T_1 profiles confirm this trend. First-order thermal perturbations remain localized near the interface, but their intensity decreases significantly compared with the strongly convective regime. These results indicate that, at $Pe = 0.5$, thermal diffusion increasingly counterbalances convective transport, leading to smoother heat-transfer processes and weaker thermal waves in both fuels.

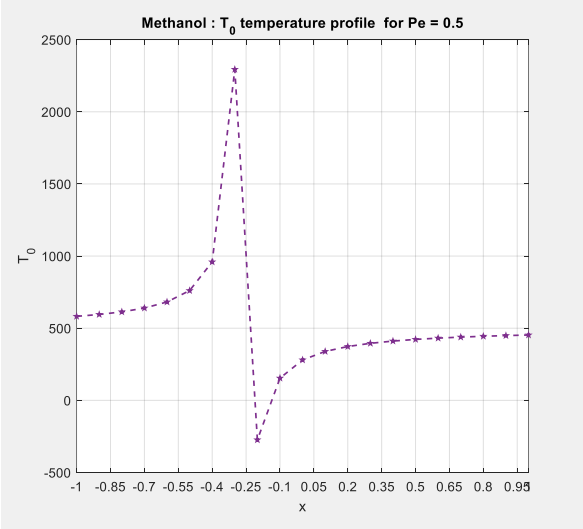

Figure 5. *$T_0(x)$ temperature profile of methanol for $P_e = 0.5$.*

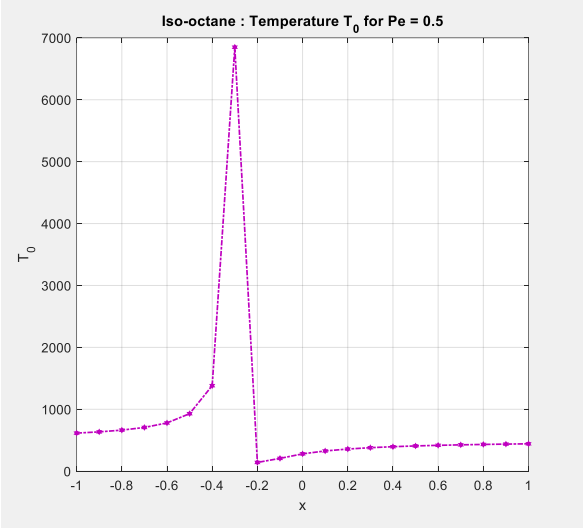

Figure 6. *$T_0(x)$ temperature profile of iso-octane for $P_e = 0.5$.*

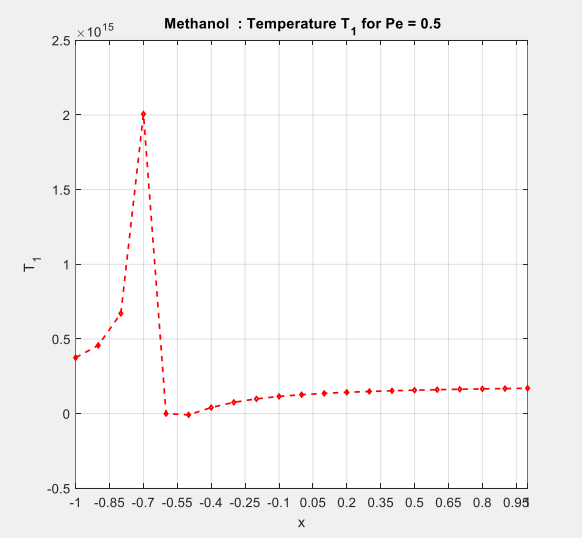

Figure 7. *$T_1(x)$ temperature profile of methanol for $P_e = 0.5$.*

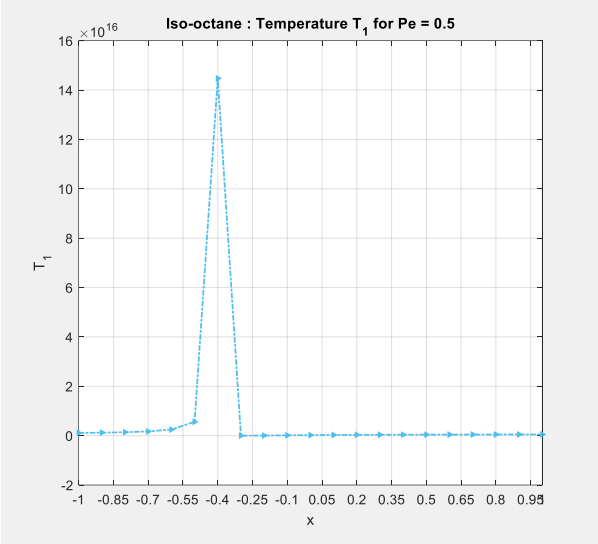

Figure 8. $T_1(x)$ *temperature profile of iso-octane for* $P_e = 0.5$.

4.1.3. Analysis of Temperature Gradients T_0 and T_1 for $Pe = 0.005$

For Pe = 0.005, the thermal waves observed at higher Peclet numbers remain present, but their intensity decreases significantly. Temperature gradients become less localized and extend over a wider region around the liquid–vapor interface, indicating the predominance of diffusive transport over convective effects. Compared with the $Pe = 5$ and $Pe = 0.5$ cases, the amplitudes of the T_0 and T_1 peaks are lower and the thermal boundary layers are more extended. Heat is therefore redistributed more uniformly within both the droplet and the surrounding gas phase, limiting the development of strong thermal heterogeneities near the interface.

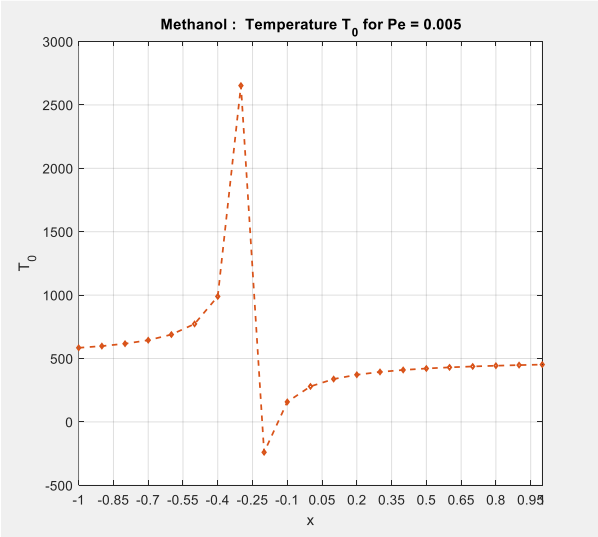

Figure 9. $T_0(x)$ *temperature profile of methanol for* $P_e = 0.005$.

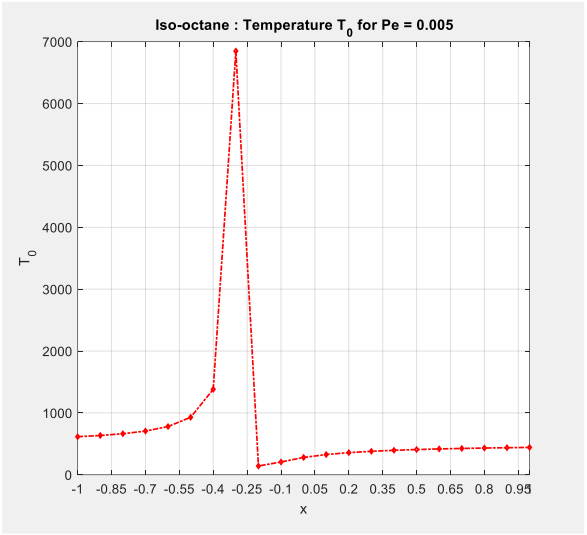

Figure 10. $T_0(x)$ *temperature profile of iso-octane for* $P_e = 0.005$.

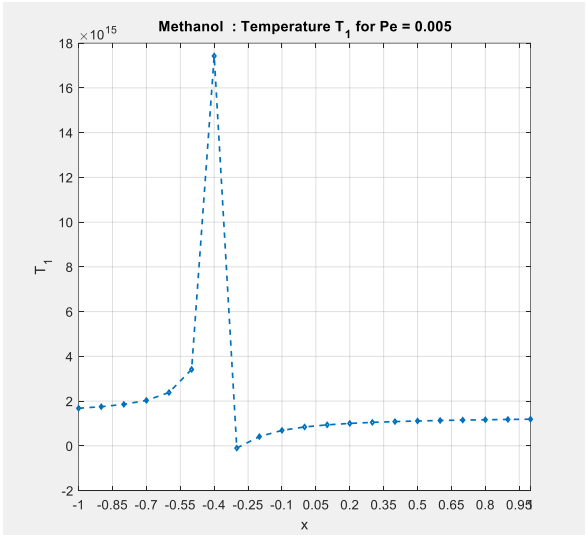

Figure 11. $T_1(x)$ *temperature profile of methanol for* $P_e = 0.005$.

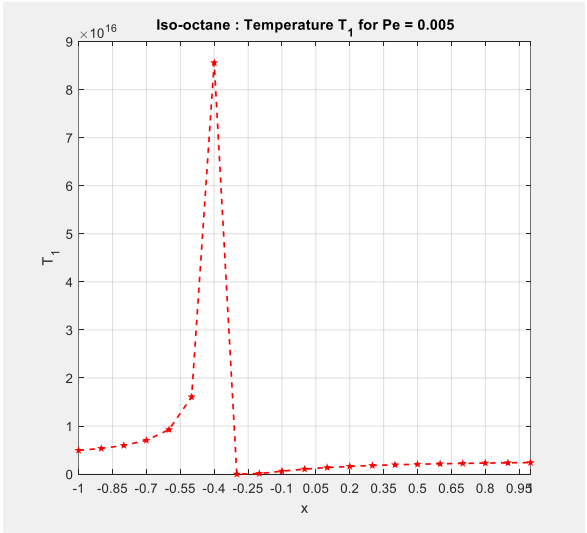

Figure 12. $T_1(x)$ *temperature profile of iso-octane for* $P_e = 0.005$.

The methanol and iso-octane profiles retain the trends observed previously, with iso-octane still exhibiting higher temperature gradients than methanol. However, the difference between the two fuels becomes less pronounced as diffusive effects become dominant. These results show that, at $Pe = 0.005$, diffusive mechanisms largely control heat transfer. The temperature gradients are weaker and more spatially distributed than those observed for $Pe = 0.5$ and $Pe = 5$, reflecting a more homogeneous redistribution of heat within the droplet and the surrounding gas phase. The temperature profiles T_0 and T_1 reveal the formation of thermal waves localized near the liquid–vapor interface during the evaporation of methanol and iso-octane droplets. The intensity and spatial extent of these thermal disturbances are strongly governed by the Peclet number. For high Peclet numbers ($Pe = 5$), convective transport dominates diffusion, leading to intense and highly localized thermal gradients. Under these conditions, iso-octane exhibits stronger thermal waves than methanol because its lower volatility requires a larger heat input for evaporation. As the Peclet number decreases ($Pe = 0.5$ and $Pe = 0.005$), diffusive transport becomes progressively dominant. The thermal gradients weaken, the thermal boundary layer becomes thicker, and heat is redistributed more uniformly throughout the droplet and the surrounding gas. Consequently, the amplitude of the thermal waves decreases and the temperature field becomes more homogeneous. Although iso-octane consistently exhibits larger thermal gradients than methanol, the differences between the two fuels diminish as diffusion becomes predominant. Overall, the results demonstrate that the Peclet number controls the balance between convective and diffusive heat transfer mechanisms and, therefore, governs the development of thermal waves during subcritical droplet evaporation. The temperature profiles obtained from the asymptotic expansion must be interpreted in accordance with the order of approximation. In particular, the first- and second-order contributions should not be interpreted independently as physical temperature fields.

4.2. Density Field Model

Figures 13–24 present the spatiotemporal evolution of the density fields $\rho_0$and $\rho_1$for methanol and iso-octane droplets subjected to different Peclet numbers ($Pe = 5$, $Pe = 0.5$, and $Pe = 0.005$). These results provide insight into the influence of convective and diffusive mechanisms on mass transfer during the evaporation process. The ρ_0 and ρ_1 profiles reveal the formation of mass waves mainly localized within the liquid phase, near the liquid–vapor interface. These structures indicate the presence of strong concentration gradients associated with vaporization and confirm the strong coupling between heat and mass transfer phenomena. The intensity and spatial extent of these waves depend strongly on the Peclet number. The following sections examine their evolution under the different transport regimes considered.

4.2.1. Analysis of Density Fields ρ_0 and ρ_1 for $Pe = 5$

According to Figures 13-16, the ρ_0 and ρ_1 profiles reveal the presence of intense mass waves in the vicinity of the liquid–vapor interface. The predominance of convective mechanisms at $Pe = 5$ strengthens concentration gradients and promotes local vapor accumulation. The amplitudes are higher for iso-octane than for methanol, indicating more localized mass transfer processes. These observations are consistent with the findings of Abramzon and Sirignano [18] and Sazhin [1].

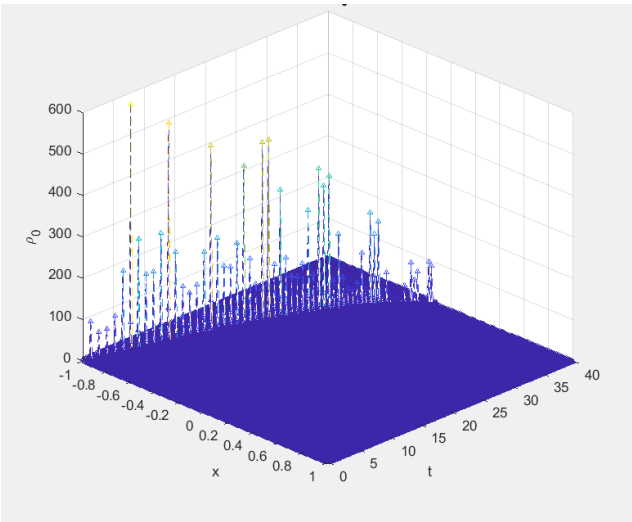

Figure 13. *Evolution of the density $\rho_0(x,t)$ field of methanol for $P_e = 5$.*

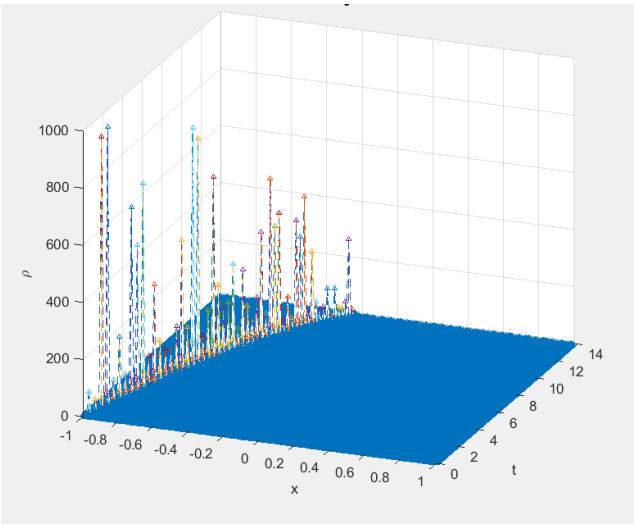

Figure 14. *Evolution of the density $\rho_0(x,t)$ of iso-octane for $P_e = 5$.*

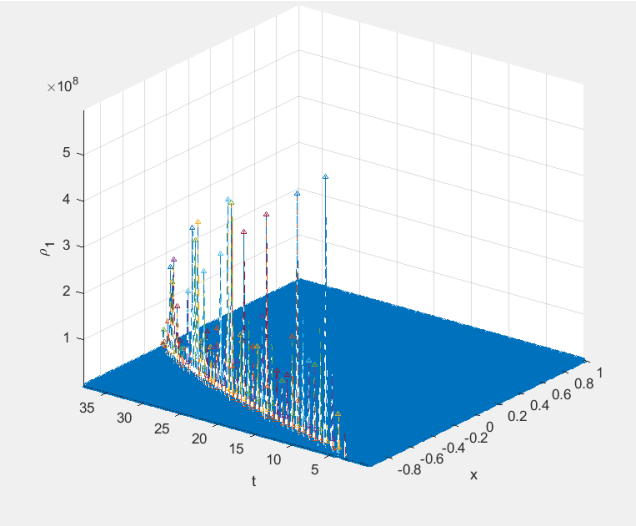

Figure 15. *Evolution of the density* $\rho_1(x,t)$ *of methanol for* $P_e = 5$.

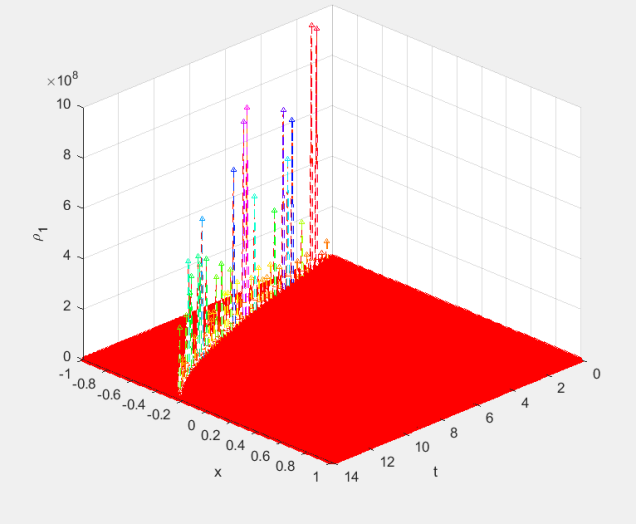

Figure 16. *Evolution of the density* $\rho_1(x,t)$ *of iso-octane for* $P_e = 5$.

The amplitudes of ρ_0 and ρ_1 remain larger for iso-octane than for methanol, confirming a stronger localization of mass transfer near the interface. The correspondence between regions of high thermal and mass gradients further highlights the thermo-mass coupling governing the evaporation process. At $Pe = 5$, convective effects therefore promote the development of both intense thermal and mass waves.

4.2.2. Analysis of Density Fields ρ_0 and ρ_1 for $Pe = 0.5$

The ρ_0 and ρ_1 profiles still exhibit mass waves localized near the liquid–vapor interface. However, their amplitudes are significantly lower than those observed at $Pe = 5$, indicating a weakening of concentration gradients within the droplet. The decrease in the Peclet number enhances diffusive transport and limits the local accumulation of vapor observed under strongly convective conditions. As a result, the mass waves become less intense and their propagation inside the droplet is reduced. This behavior is consistent with the thermal field results and confirms that decreasing the Peclet number progressively attenuates the thermo-mass transfer instabilities associated with the evaporation process.

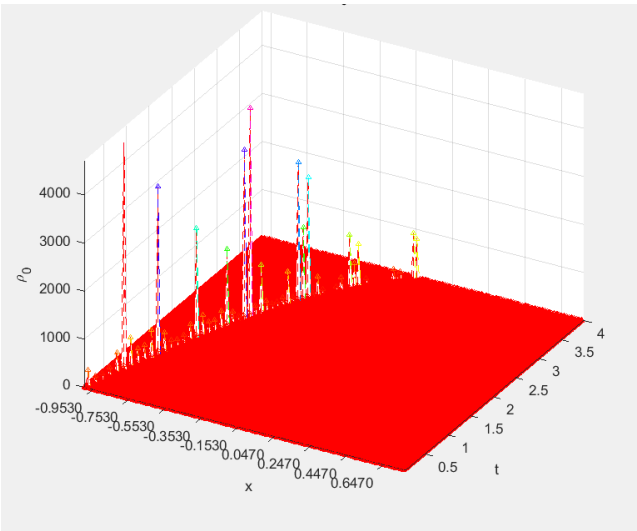

Figure 17. *Evolution of the density* $\rho_0(x,t)$ *of methanol for* $P_e = 0.5$.

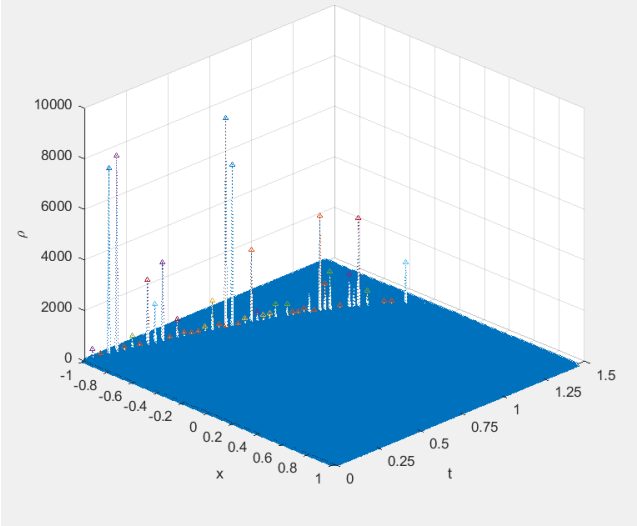

Figure 18. *Evolution of the density* $\rho_0(x,t)$ *of iso-octane for* $P_e = 0.5$.

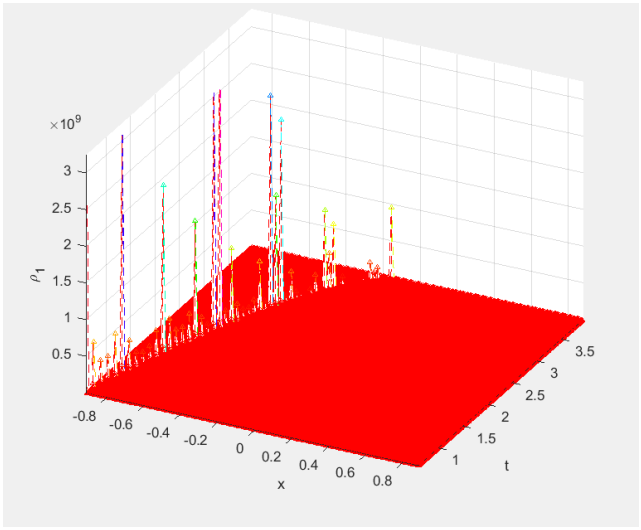

Figure 19. *Evolution of the density $\rho_1(x,t)$ of methanol for $P_e =$ 0.5.*

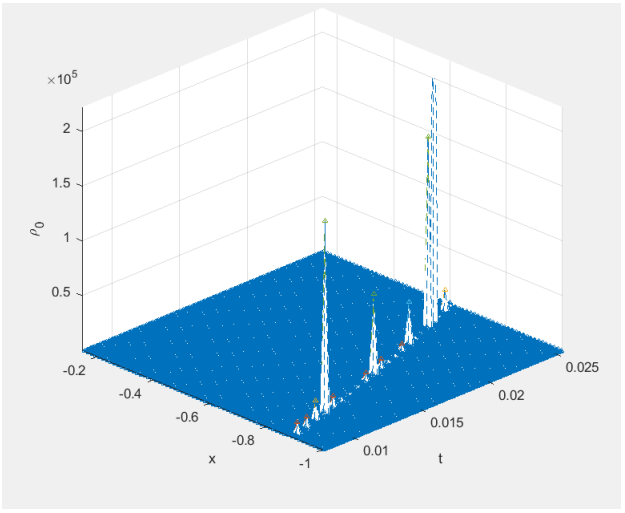

Figure 21. *Evolution of the density $\rho_0(x,t)$ of methanol for $P_e =$ 0.005.*

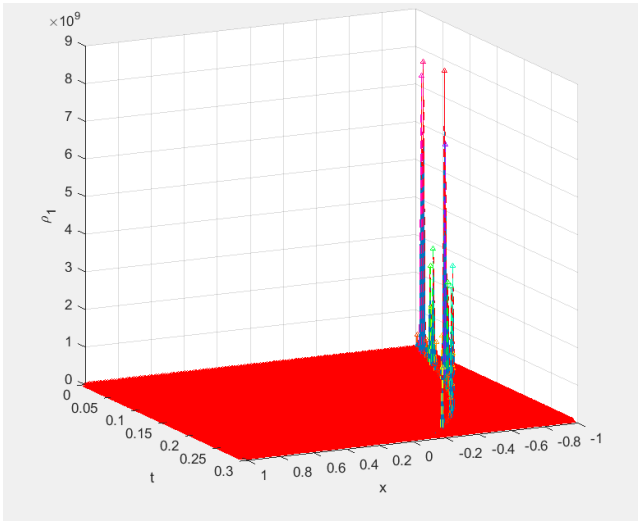

Figure 20. *Evolution of the density $\rho_1(x,t)$ of iso-octane for $P_e =$ 0.5.*

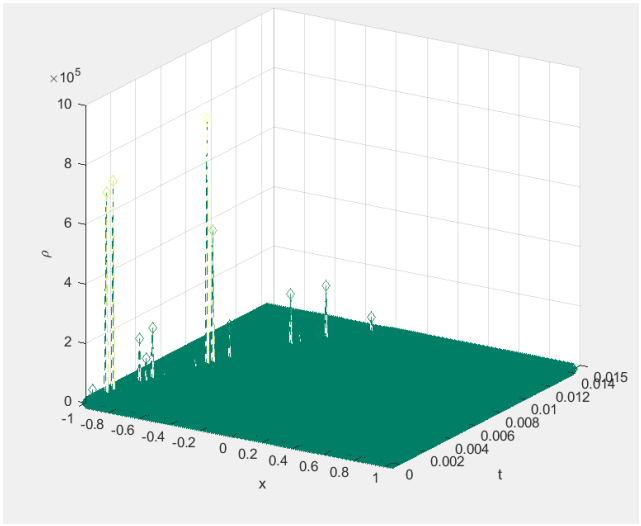

Figure 22. *Evolution of the density $\rho_0(x,t)$ of iso-octane for $P_e =$ 0.005.*

4.2.3. Analysis of Density Fields ρ_0 and ρ_1 for $Pe = 0.005$

For $Pe = 0.005$, density fluctuations remain localized near the liquid–vapor interface, but their amplitudes are significantly lower than those observed for $Pe = 5$ and $Pe = 0.5$. The discontinuities appearing in the ρ_0 and ρ_1 profiles rapidly decay, and their propagation within the liquid phase becomes limited. This behavior reflects the predominance of diffusive mechanisms, which promote a more uniform redistribution of mass within the droplet and reduce the local vapor accumulation responsible for the strong discontinuities observed at higher Peclet numbers. The methanol and iso-octane profiles retain the same qualitative trends as in the previous cases, although with weaker amplitudes and smoother gradients.

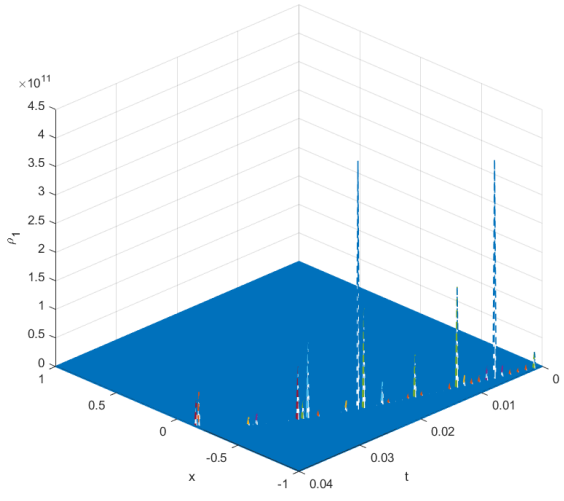

Figure 23. *Evolution of the density $\rho_1(x,t)$ of methanol for $P_e =$ 0.005.*

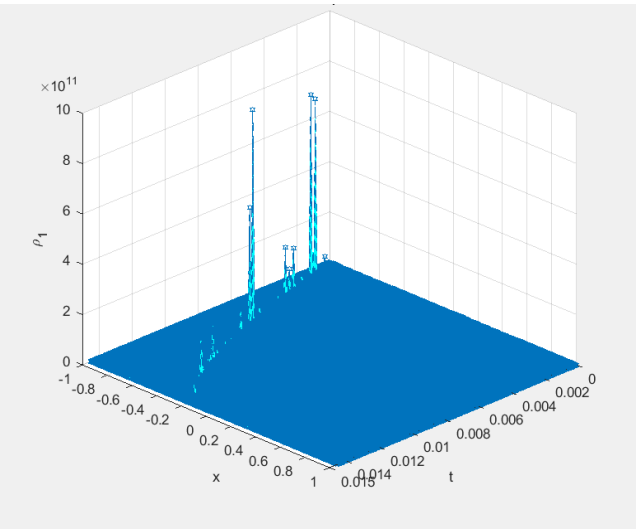

Figure 24. *Evolution of the density $\rho_1(x,t)$ of iso-octane for $P_e =$ 0.005.*

disturbances within the droplet and promote a more homogeneous evaporation process.

4.3. Droplet Radius Evolution

Figures 25 and 26 present the temporal evolution of the normalized squared droplet diameter of methanol for different Peclet numbers. The regression curves exhibit an approximately linear decrease with time, consistent with the classical d^2-law of droplet evaporation, indicating an almost constant evaporation rate over the considered period. The droplet lifetime is determined from the regression law by identifying the time at which the predicted droplet radius vanishes.

Table 2 summarizes the predicted droplet lifetimes for the three investigated Péclet numbers. The results reveal a strong dependence of evaporation dynamics on the transport regime. Specifically, the droplet lifetime increases with increasing Péclet number, with Pe = 5 corresponding to the longest lifetime and Pe = 0.005 to the shortest.

Table 2. *Reported lifetime of methanol droplet.*

$t/(d_0)^2$	$P_e = 5$	$P_e = 0.5$	$P_e = 0.005$
s/mm^2	40	4	0.04

The reported lifetime trends are interpreted as analytical predictions within the adopted assumptions.

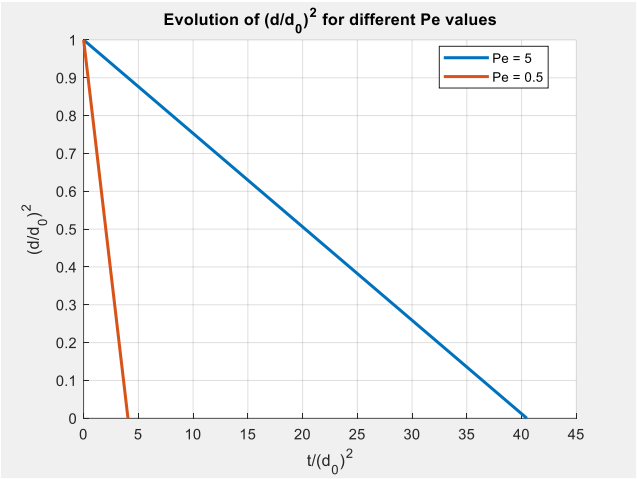

Figure 25. *Temporal evolution of the squared droplet diameter (order 0) of methanol for different Peclet numbers.*

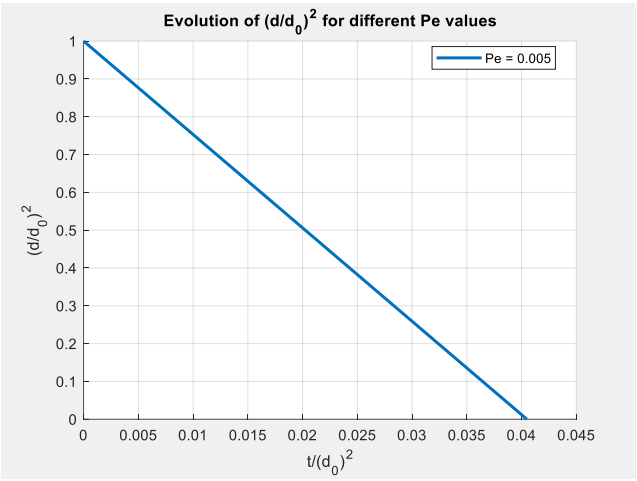

Figure 26. *Temporal evolution of the squared droplet diameter for $Pe = 0.005$.*

The results indicate that droplet lifetime increases with the Peclet number. The case corresponding to $Pe = 5$ exhibits the slowest diameter regression, whereas lower Peclet numbers lead to faster evaporation and shorter lifetimes. This behavior is consistent with the transport mechanisms identified from the density and temperature field distributions. At high Pe, convection promotes strong thermal and mass gradients near the liquid–vapor interface, slowing the homogenization of heat and vapor within the droplet. As Pe decreases, diffusion becomes dominant, enhancing internal transport and accelerating evaporation process. Consequently, evaporation proceeds more rapidly and the droplet lifetime decreases.

These results demonstrate that the Peclet number is a key parameter governing droplet evaporation. Lower values of Pe promote more homogeneous transport processes and significantly reduce droplet lifetime, whereas higher values maintain stronger thermo-mass transfer heterogeneities and prolong the evaporation process.

The present results are analytical predictions obtained under the assumptions of the proposed model. No independent numerical or experimental validation is provided in this study. Consequently, the predicted temperature, density, and evaporation lifetime trends should be interpreted within the limits of the adopted formulation.

5. Conclusion

This study investigated the influence of the Peclet number on the evaporation of methanol and iso-octane droplets under subcritical conditions using a first- and second-order analytical solution of the Navier–Stokes equations. The results show that the Peclet number strongly governs the thermal and mass transfer structures developing near the liquid–vapor interface. For high Peclet numbers, convective transport dominates, promoting the formation of intense thermal and mass waves associated with large temperature and concentration gradients. In contrast, as the Peclet number decreases, diffusive mechanisms become predominant, progressively attenuating these disturbances and leading to a more homogeneous redistribution of heat and mass within the droplet. The analysis also highlights significant differences between the two fuels. Iso-octane exhibits stronger thermal and mass gradients than methanol, indicating a greater localization of transport processes near the interface. A major outcome of this work is the demonstrated influence of the Peclet number on droplet lifetime. High Peclet numbers tend to prolong the evaporation process by enhancing thermo-mass transfer heterogeneities, whereas low Peclet numbers promote more uniform transport and accelerate droplet disappearance. Consequently, decreasing the Peclet number leads to a significant reduction in the lifetime of both methanol and iso-octane droplets. These findings demonstrate that the Peclet number is a key parameter governing dynamic evaporation under subcritical conditions. They provide new insight into the interplay between convection and diffusion in the formation of thermo-mass transfer waves and in the control of droplet lifetime, with potential applications in the optimization of atomization, evaporation, and combustion processes.

The present analysis is based on an asymptotic analytical formulation under spherical symmetry, uniform pressure, thermodynamic equilibrium at the interface, and constant thermophysical properties within each approximation order. Experimental validation and direct numerical simulations were not conducted in this work. Therefore, the predicted thermal and density disturbances should be interpreted as analytical predictions within the framework of the adopted model. Future studies will focus on quantitative validation against numerical simulations and experimental data.

Nomenclature

Symbol	Definition	Unit
r'	Radial Distance from Droplet Center	m
$R'(t)$	Instantaneous Droplet Radius	m
$u'(r',t')$	Radial Velocity Component	$m.s^{-1}$
t'	Time	s
T	Temperature	K
P	Pressure	Pa
ρ	Density	$kg.m^{-3}$
C_p	Specific Heat at Constant Pressure	$J.kg^{-1}.K^{-1}$
λ	Thermal Conductivity	$W.m^{-1}\cdot K^{-1}$
t_{res}	Droplet Lifetime	s
t_{dif}	Diffusion Time Scale	s

Author Contributions

Yendoubouame Lare: Conceptualization, Data curation, Investigation, Methodology, Software, Visualization, Writing – original draft

Koffi Sagna: Conceptualization, Data curation, Methodology, Supervision, Validation, Writing – review & editing

Conflicts of Interest

The authors declare no conflicts of interest.

References

[1] Sazhin, Sergei S., "Advanced models of fuel droplet heating and evaporation," *Progress in Energy and Combustion Science*, vol. 32, p. 162–214, 2006.

[2] Maxwell, J. C., "Diffusion," in *Encyclopaedia Britannica, ninth ed*, 1877.

[3] D. B. Spalding, "Theory of particle combustion at high pressures," *ARS J*, vol. 29, pp. 828-835, 1959.

[4] GODSAVE, G. A. E., "Studies of the combustion of drops in a fuel spray the burning of single drops of fuel," in *in Fourth Symposium on Combustion*, 1953.

[5] S. Saengkaew, T. Charinpanikul, C. Laurent, Y. Biscos, G., "Processing of individual rainbow signals," *Exp. Fluids*, vol. 48, pp. 111-119, 2010.

[6] S. Saengkaew, D. Bonin, P. Briard, and G. Grehan, " Pulsed-beam global rainbow refractometry: Estimation of concentrations and inter-particle distances," in *Francophone Congress on Laser Techniques (CFTL2010)*, Vandoeuvre-l ès-Nancy (France), 2010.

[7] Yendoubouame Lare, Koffi Sagna, Kodjo S. Apeke, Dzidula K. Afodanyi, Yendoube Lare, and Amah S. d'Almeida, "Study of the Thermodynamic Properties of a Drop in an Environment under Subcritical Conditions During Evaporation," *International Journal of Physics*, vol. 11, no. 3, pp. 97-105, 2023.

[8] Koffi Sagna, Amah D'Almeida, "A Study of Droplet Evaporation," *American Journal of Modern Physics*, vol. 2, pp. 71-76, 2013.

[9] Koffi Sagna, Komi Apelete Amou, Tchamye Tcha-Esso Boroze, Djima Kassegne, Amah d'Almeida, Kossi Napo, "Environmental Pollution due to the Operation of Gasoline," *International Journal of Oil, Gas and Coal Engineering Engines: Exhaust Gas Law*, vol. 5, no. 4, pp. 39-43, 2017.

[10] Sagna Koffi, " Study of the evaporation of an isolated liquid droplet at subcritical and supercritical pressures," Universit éde Lom é, Lom é, 2014.

[11] Koffi Sagna, Amah D'Almeida, "Supercritical Evaporation of a Drop," *International Journal of Research in Engineering and Science (IJRES)*, vol. 2, no. 7, pp. 41-47, July. 2014.

[12] Sanchez-Tarifa C., Crespo A., Fraga E., "Theoretical model for the combustion of droplets in super-critical conditions and gas pockets," *Astronautica Acta*, vol. 17, pp. 685-692, 1972.

[13] Manuel Arias -Zugasti, Pedro L. Garcia -Ybarra & Jose L. Castillo, "Unsteady Effects in droplet vaporisation lifetimes at subcritical and supercritical conditions," *Combust. Sci. and Tech*, vol. 153, pp. 179-191, 2000.

[14] D'ALMEIDA, PRUD'HOMME, " Droplet evaporation: laws governing the recession of the radius," 19th French Congress of Mechanics, Marseille, 2009.

[15] Theodore L. Bergman; Adrienne S. Lavine; Frank P. Incropera; David P. Dewitt, Fundamentals of Heat and Mass Transfer, Jefferson City: John Wiley & Son, 2011.

[16] Sirignano, W. A, "Fluid Dynamics and Transport of Droplets and Sprays," *Cambridge University Press, Cambridge*, 2010.

[17] J. Schwarz, J. Smolik, J. Kugler, J. Egama, "Evaporation of methanol droplet at high ambient temperatures," *Journal of Aerosol Science*, Vols. 26, Suppl 1, pp. 271-272, 1995.

[18] B. Abramzon and W. A. Sirignano, "Droplet vaporization model for spray combustion calculations.," *International Journal of Heat and Mass Transfer*, vol. 32, no. 9, p. 1605–1618, 1989.

[19] Abgail P. Pinheiro, Joao Marcelo Vedovoto, "Evaluation of Droplet Evaporation Models and the Incorporation of Natural Convection Effects," *Flow, Turbulence and Combustion*, 2018.

Biography



Yendoubouame Lare is a PhD candidate in Applied Physics at the University of Lom é, Togo. His research focuses on thermodynamics, heat and mass transfer, fluid mechanics, and the numerical modeling of transport phenomena. His doctoral work investigates the evaporation dynamics of liquid droplets under subcritical and supercritical conditions, with particular emphasis on the influence of thermophysical parameters on heat and mass transfer mechanisms. His scientific interests encompass multiphase flows, droplet evaporation, computational fluid dynamics, and energy systems. Through his research activities, he contributes to the advancement of knowledge in thermal sciences and transport phenomena, with applications in energy efficiency, combustion systems, and aerospace engineering.



Koffi Sagna is an Associate Professor in the Department of Physics at the Faculty of Sciences, University of Lome, Togo. Specializing in materials physics, fluid mechanics, and energetics, his research primary focuses on thermodynamic modeling, numerical simulations, and transport phenomena. He is particularly renowned for his work on the thermodynamic properties and evaporation processes of isolated droplets under critical, subcritical, and supercritical thermal environments, a crucial field for optimizing energy systems and internal combustion chambers. As a researcher at the Solar Energy Laboratory and an expert at the Regional Center of Excellence for Electricity Mastery (CERME), he supervises various doctoral research projects. His scientific contributions include numerous international publications addressing fluid dynamics, multiphase interface behaviors, and renewable energy integration.

Research Field

Yendoubouame Lare: Thermodynamics of Isolated Fluid Droplets, Numerical Simulation of Fluid Mechanics, Energy Systems and Transport Phenomena, Heat and Mass Transfer Processes, Evaporation Modeling in Critical Environments, Environmental Pollution, Thermal Engineering and Materials Physics

Koffi Sagna: Thermodynamics of Isolated Fluid Droplets, Numerical Simulation of Fluid Mechanics, Energy Systems and Transport Phenomena, Heat and Mass Transfer Processes, Evaporation Modeling in Critical Environments, Environmental Pollution, Thermal Engineering and Materials Physics